Biochar (2022) 4:14
https://doi.org/10.1007/s42773-022-00143-4

ORIGINAL RESEARCH

Impacts of temperatures and phosphoric-acid modification to the physicochemical properties of biochar for excellent sulfadiazine adsorption

Xue-Yu Zeng[1] · Yu Wang[2] · Rong-Xin Li[1] · Hai-Lei Cao[1] · Ya-Feng Li[3] · Jian Lü[1,3]

Received: 14 October 2021 / Accepted: 10 February 2022

Abstract

The textural properties and surface chemistry of phosphoric acid-modified biochars (PABCs) prepared at different pyrolysis temperatures (500–700 °C) were studied based on the results obtained from XRD, SEM, BET, FT-IR, Raman, XPS and elements analyses. PABCs prepared at higher temperatures tended to possess a bigger proportion of microporous structure. The adsorption capacity and initial rate of PABCs for sulfadiazine (SDZ) were notably improved to 139.2 mg/g and 9.66 mg/(g min) as calculated from the Langmuir model. The adsorption equilibrium time was only one quarter of that without modification. The H_3PO_4 modification was advantageous to produce phosphate and break functional groups to form disordered carbon structure abundant of micropores. The enhancement in the adsorption of SDZ was due to the confinement effect of hydrophobic cavities from the mircoporous structure and the π–π electron–donor–acceptor interaction. Specially, PABCs exhibited stable adsorption capacities at a wide pH range (3.0–9.0) or relatively high concentrations of coexisting ions.

Highlights

- Phosphoric acid breaks functional groups to form disordered carbon and surface phosphate;
- The q_m of PABCs for sulfadiazine reached 139.2 mg/g that was competitive to MWCNTs;
- The hydrophobicity of PABCs and π–π EDA interaction played a leading role for binding SDZ

Keywords Coffee grounds-derived biochar · Pyrolysis · Surface modification · Sulfadiazine adsorption · Micropore structure

1 Introduction

Antibiotics are one class of the most prevalent contaminants, which have been widely used in the pharmaceutical, medical and aquacultural industries (Martucci et al. 2014; Zheng et al. 2013). These contaminants have given rise to serious environmental problems due to their refractory and toxicity (Bougnom and Piddock 2017). Sulfonamides (SAs) have a high detection rate in the sewage, water, soil, surface water all over the world because of their large amount of application (Kummerer 2002; Nakata et al. 2005; Yan et al. 2018). They would induce the generation of drug-resistant bacteria (Bai et al. 2014; Davies and Davies 2010; Kim et al. 2014), and cause hypoimmunity and dysbacteriosis after entering

✉ Hai-Lei Cao
caohailei@163.com

[1] Fujian Provincial Key Laboratory of Soil Environmental Health and Regulation, College of Resources and Environment, Fujian Agriculture and Forestry University, Fuzhou 350002, China

[2] Anhui Pushi Ecological Environment Engineering Co., Ltd., Hefei 230000, China

[3] State Key Laboratory of Photocatalysis on Energy and Environment, Fuzhou University, No. 2 Xue Yuan Road, Fuzhou 350116, China

Published online: 22 February 2022

the human bodies through food chain (Lange and Dietrich 2002; Poloni et al. 2017). Therefore, it is urgent to search for advanced technologies to remove these refractory antibiotics from water.

Many effective technologies, such as chemical remediation, advanced oxidation, photocatalysis and adsorption have been developed and applied to remove antibiotics (Zessel et al. 2014). Among these approaches, adsorption has become one of the most widely accepted technologies due to its economy, feasibility and environmental–friendliness (Gao et al. 2012; Hu et al. 2020; Kim et al. 2020; Ling et al. 2016; Xiao et al. 2018). Based on the characteristics of high porosity, hydrophobicity and aromaticity (Peiris et al. 2017), biochars (BCs) have attracted extensive attention as an excellent adsorbent for removing organic contaminants (Dai et al. 2020; Hopkins and Hawboldt 2020; Ndoun et al. 2020; Tan et al. 2015; Yao et al. 2020). BCs are the pyrolysis products of biomasses at low temperatures (< 800 °C) in the oxygen-limited environment (Tripathi et al. 2016). Among those raw materials from agriculture for the preparation of BCs, coffee is one of the world's most traded products with an annual output of more than 8.0 billion kg per year (Vardon et al. 2013). The solid residues (coffee grounds, denoted as CGs) containing 40% lignin (Jeguirim et al. 2014) are easy to polycondensate to form a polycyclic aromatic hydrocarbon structure, and thus are believed to be the potential to exhibit a higher fixed carbon content under hyperthermal conditions (Ma et al. 2015).

On top of all the factors that might affect the physicochemical properties of BCs (Antonangelo et al. 2019; Suliman et al. 2016), the pyrolysis temperature is a key parameter that would affect the quantity of functional groups, porosity and aromaticity level of biochar (Choi and Kan 2019). The dissociation energy required to decompose the functional groups is different owing to the distinct functionalities contained in biomass (Angin and Sensoz 2014; Gao et al. 2021; Li et al. 2019). It remains a challenge to reveal the relationship between the temperature and the biochar quality because of the various nature and composition of biomasses.

Furthermore, various modification strategies including acid and alkaline activation (Bashir et al. 2018; Guo et al. 2017; Vithanage et al. 2015; Wang and Kaskel 2012), electrochemical modification (Yang et al. 2019a), magnetic modification (Quah et al. 2020), mineral modification (Oginni et al. 2020), and oxidant modification (Huff and Lee 2016), have been applied to improve the adsorption performance of biochar. The combined alkali-acid modification can significantly improve the adsorption capacity of BCs, because the former alkali treatment could help to produce more activated sites for the latter acid modification (Tang et al. 2018), and thus not only expand the porosity of the original biochar, but also increase the number of acid binding sites and oxygen functional groups (Wang and Wang 2019). In particularly, H_3PO_4 acidification after the alkali treatment could optimize pore size distribution, and would be beneficial for the specific surface area increasing as well as the pore volume (Liu et al. 2012). Moreover, the enriched functional groups, P=O and P=OOH for example, could impact the charge distribution of the adsorbent and the H-bonding formation thanks to the lone pair electrons, and therefore tend to lead to the stronger surface complexation for adsorption (Peng et al. 2017). Compared to sulfuric acid, nitric acid, zinc chloride and other modification methods, phosphoric acid modification can protect the carbon skeleton and exhibit greater advantages in micropore formation (Chen et al. 2018; Kang et al. 2018; Liu et al. 2020a). Moreover, considering their environmental effect, equipment corrosion and chemical recovery, phosphoric acid is most preferred (Chu et al. 2018; Prahas et al. 2008). To our knowledge, there has been no report on the synergistic modification of biochar through combined alkaline and phosphorous acid treatment.

Herein, we aim to prepare a series of H_3PO_4-modified coffee grounds-derived activated biochar (PABC) materials for removing sulfadiazine (SDZ) in aqueous solutions. The effects of pyrolysis temperature and phosphoric acid modification on the adsorption performance of biochar were systematically explored in the first place.

2 Materials and methods

2.1 Chemicals and reagents

Chemicals used in this work were of reagent-grade and were dissolved in deionized water. SDZ (98%), KOH, HCl and H_3PO_4 were purchased from Aladdin (Shanghai, China).

2.2 Adsorbents preparation

Coffee grounds (CGs) were collected from the Starbucks located in Fuzhou City, Fujian Province, China. CGs were washed with 75% ethanol and then dried in an oven at 60 °C for 12 h. After being dried, CGs were screened by 100 mesh sieve. The pre-treated CGs were calcined in a tube furnace (GSL-1500X, China) for 1 h under N_2. CGs pyrolyzed at 500 °C, 600 °C and 700 °C were labelled as CBC-500, CBC-600 and CBC-700, respectively. Then, the CBCs were activated with two equivalents of KOH at 700 °C for 1 h to obtain activated carbon ABC-500, ABC-600 and ABC-700. The ABCs were washed with hydrochloric acid (0.1 M) and deionized water until the pH of the filtrate equaled 7.0.

PABCs were prepared as follows: ABCs were firstly mixed with 35.0 wt% phosphoric acid at a mass ratio of 1:2, and then immersed for 30 min before being sonicated for 10 min. This process was repeated for 6 times. After that,

the H_3PO_4-modified sample was repeatedly washed with deionized water until the pH value of the eluate was about 7.0. After being dried overnight at 60 °C in an oven, PABCs were prepared and denoted as PABC-500, PABC-600 and PABC-700, respectively.

2.3 Characterization

The surface morphology was obtained by scanning electron microscope (SEM, ProX Premium, Phenom, Netherlands). Powder X-ray diffraction (PXRD) was carried out on a diffractometer (Miniflex 600, Rigaku, Japan) with Cu Kα radiation (λ = 0.154 nm). The Raman spectra were measured on a Raman spectrometer (LabRAM HR800, HORIBA Jobin Yvon, France) using 633 nm laser. The N_2 adsorption/desorption isotherms, surface area and porous properties were determined by the Brunauer–Emmett–Teller method (BET, ASAP2460, Micromeritics, USA) at liquid nitrogen temperature (77 K). The carbon (C), hydrogen (H), and nitrogen (N) contents of each biochar sample were evaluatedusing an Elemental Analyzer (Vario max cube, Elementar, Germany). X-ray photoelectron spectroscopy (XPS, ESCALAB 250Xi, Thermo Fisher, USA) served for the element composition determination with Al Kα x-ray source (15 kV, 10 mA). The functional group analysis of ABC-700 and PABC-700 was carried out by the Fourier transform infrared spectrometer (Nicolet iS50, Thermo, USA), with a spectral range of 400–4000 cm^{-1}. The zeta potential was determined using a high sensitivity Zeta potential analyzer (NanoBrook Omni, Brookhaven, USA). Thermogravimetric analysis was performed using a thermogravimetric analyzer (TG 8120, Rigaku, Japan) at a heating rate of 10 °C/min, and a nitrogen flow rate of 100 mL/min. A drop shape analyzer (DSA100, Krüss GmbH, Germany) was employed to observe the contact angle (CA) of biochar samples.

2.4 Batch adsorption experiments

In a typical batch adsorption experiment, 5.0 mg adsorbent was added to 50 mL SDZ solution (10 mg/L) shaking in a water bath thermostatic oscillator (25 °C, 130 r/min), and sampled for the determination of SDZ concentration using a UV–vis absorbance (UV-2600, Shimadzu, Japan) at 246 nm. The standard curves of SDZ determined at various pH values were demonstrated in Fig. S1.

Similarly, the adsorption isotherms were measured by adding 5.0 mg adsorbent to a range of concentrations (1–20 mg/L) of SDZ solutions and shaking in a water bath thermostatic oscillator (25 °C, 130 r/min) for 720 min.

The amount of SDZ adsorbed at equilibrium (q_e (mg/g)) was calculated by the following equation (Eq. (1)):

$$q_e = (C_0 - C_e)V/W, \tag{1}$$

where q_e (mg/g) is the adsorption capacity of an antibiotic. C_0 (mg/L) and C_e (mg/L) indicate the initial concentration and equilibrium concentration, respectively. V (L) is the volume of reaction solution and W (g) is the mass of the adsorbent.

Pseudo-second-order kinetic model (Eq. (2)) (Ho 2006) was represented asfollows:

$$t/q_t = 1/k_2 q_e^2 + t/q_e = 1/h + t/q_e, \tag{2}$$

where q_t (mg/g) is the adsorption amount at time t. k_2 (g/(mg min)) is the rate constant determined by the t/q_t versus t, and $h$indicates the initial adsorption rate.

The Langmuir (Eq. (3)) (Yang et al. 2017) and Freundlich (Eq. (4)) (Yao et al. 2011) isotherm models are shown below:

$$q_e = q_m K_L C_e / \left(1 + K_L C_e\right), \tag{3}$$

$$q_e = K_F C_e^{1/n}, \tag{4}$$

where q_m (mg/g) is the maximum adsorption capacity. C_e (mg/L) is the solution equilibrium concentration. K_L is the Langmuir constant; K_F and n are the Freundlich constant.

3 Results and discussion

3.1 Physical and chemical properties of the synthetic carbonaceous materials

SEM (Fig. 1a–i) illustrated the morphology changes of the biochars under different treatments. It could be clearly seen that initial biochars possessed smooth surface, and limited pore structures were observed. After KOH activation, the surface of ABCs became rough and collapsed which should be ascribed to the etching effect of alkali vapor. Furthermore, it was obvious that roughly porous structures were revealed on the surface of PABCs after the modification by H_3PO_4.

As depicted in the XRD pattern (Fig. 2a), two obvious broad peaks were discovered at 2θ = 24.2° and 43.4° for PABCs prepared at various pyrolysis temperatures. These two peaks were supposed to be assigned to the (002) and (100) crystal planes of graphite carbon. The intensity of the peak at 24.2° decreased along with the rise of the temperature, which was an implication of the increase of the disordered carbon along withthe reduced degree of graphitization (Zhang et al. 2019).

Moreover, the PABC-700 showed a relatively weak intensity at 24.2° compared to ABC-700. It was evident

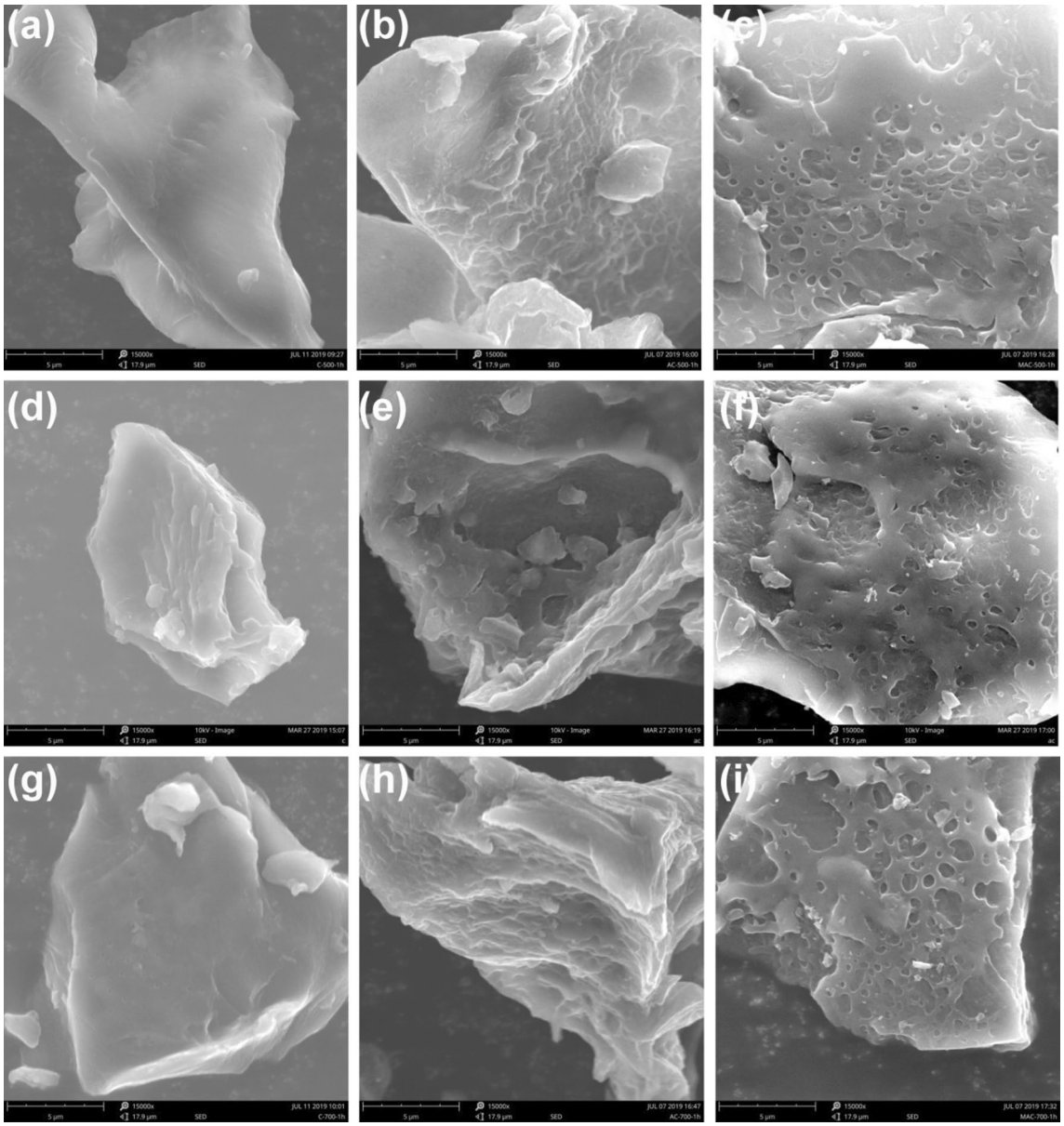

Fig. 1 SEM patterns of **a** CBC-500; **b** ABC-500; **c** PABC-500; **d** CBC-600; **e** ABC-600; **f** PABC-600; **g** CBC-700; **h** ABC-700; and **i** PABC-700 (×15,000 magnification)

that the H_3PO_4 modification was propitious to form disordered carbon at the fixed pyrolysis temperature. In addition, the decrease of I_D/I_G from 1.502 for ABC-700 to 1.460 for PABC-700 as calculated from the Raman shift (as shown in Fig. 2b) conveyed that abundant functional groups existed on the external surface and some surface defects were occupied after phosphorous acid modification (Deng et al. 2015).

A type I adsorption isotherm was discovered as shown in Fig. 3 based on the analysis from the adsorption/desorption of the N_2. According to Table 1, both the BET surface areas and pore volume of PABCs were enlarged compared with ABCs prepared at related pyrolysis temperatures, and thus PABCs showed a superior porosity to ABCs. Notably, ABC-600 had smallest C content, BET surface area and pore volume compared with those obtained at 500 and 700℃. It was deduced that the volatiles, tars and other products produced by the pyrolysis of coffee residue at about 600 °C would block part of biochar channels (Sakhiya et al. 2020). With the further increase of pyrolysis temperature, these products would eventually decompose into volatile gases and escape, which resulted in more microporous structures, leading to an increase in pore volume (Angin et al. 2013). It should be noted that, biochar prepared at 700 °C had specific pore structures, especially the ratio of the micropore volume.

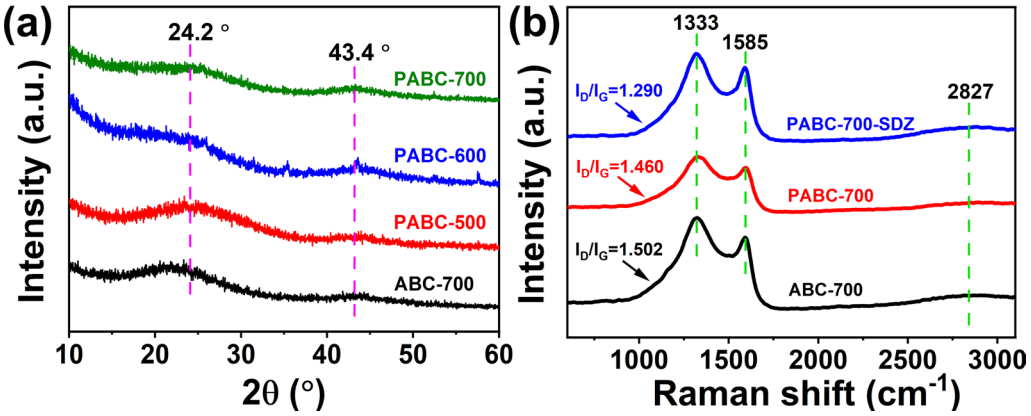

Fig. 2 **a** XRD data of ABC-700 and PABCs; **b** Raman spectra with band ratio (I_D/I_G) for ABC-700, and PABC-700 before and after adsorption of SDZ

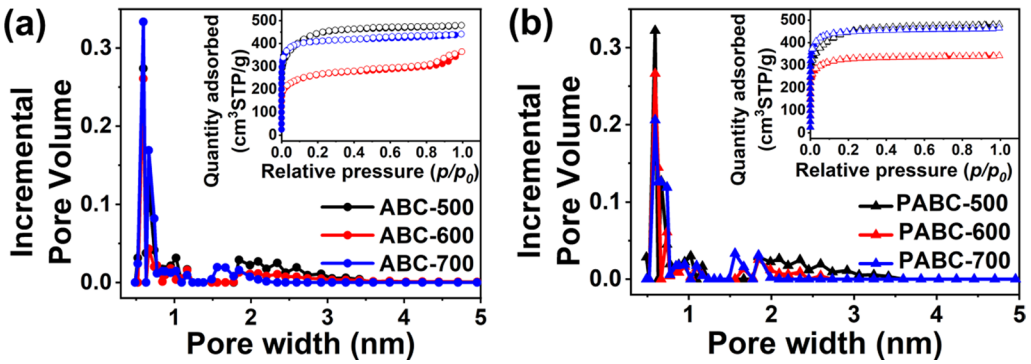

Fig. 3 Pore size distribution of **a** ABCs and **b** PABCs. Inset: N_2 adsorption/desorption isotherms

Table 1 Physical parameters of ABCs and PABCs

Sample	Contents (%)			Aromatic ratio	S_{BET} (m^2/g)	S_{mic} (m^2/g)	S_{mes} (m^2/g)	V_{total} (m^3/g)	V_{mic} (m^3/g)
	C	H	N	H/C					
ABC-500	57.37	3.20	0.44	0.67	1400	687	713	0.742	0.368
ABC-600	51.99	3.62	0.97	0.84	832	484	348	0.563	0.251
ABC-700	70.51	2.46	0.30	0.42	1253	1064	189	0.682	0.549
PABC-500	59.58	3.05	0.43	0.61	1411	706	705	0.744	0.378
PABC-600	61.86	3.17	1.21	0.61	1006	774	232	0.529	0.401
PABC-700	76.43	2.40	1.15	0.38	1365	1180	185	0.720	0.610

As shown in Table 1, the surface area and volume of the micropore in PABC-700 obtained from the BET and DFT models are approximately 1.6 times those of PABC-500, respectively. In addition, the mesoporous surface area decreased rapidly from 705 m^2/g for PABC-500 to 185 m^2/g for PABC-700, indicating the transition from mesoporous to microporous structure with the temperature increase.

Interestingly, the introduction of phosphoric acid activation (PABC-700) could further improve the S_{mic} and V_{mic} by 10% and 13% compared with ABC-700. The H/C atomic ratio (as shown in Table 1) reinforced the fact that PABC-700 exhibited the highest aromaticity among all the prepared biochar samples (Xiao et al. 2016).

The pyrolysis behaviors of PABCs were further investigated through TGA as shown in Fig. S2. The weight loss that happened before 120 °C was mainly because of the water removal. After that, PABC-500 and PABC-600 showed relatively good thermal stability until an obvious weight loss at

higher temperatures that ascribed to the decomposition of lignin was detected (Reza et al. 2020). What's more, only small amount of weight loss was detected during the whole duration for PABC-700 ,showing an extremely high thermal stability.

The expatiatory XPS spectra of major elements, including C1s and P2p were exhibited in Fig. 4b, c. Peaks at 284.8 eV, 285.8 eV and 286.8 eV were contributed by C–C, C–O and C=O, testifying the hydrophobic surface of PABC-700 (Wei et al. 2017; Zhao et al. 2016), which would be beneficial to the conductive of adsorption (Tomczyk et al. 2020). As for P2p, two peaks at 134.1 eV and 135.8 eV, attributed to P–O and P=O (Liu et al. 2017; Pan et al. 2021), were separated as an evidence for the successful introduction of phosphorus-containing groups to the surface of PABC-700 by means of phosphoric acid modification. Obviously, phosphoric acid modification made PABCs possess diversified surface functional groups. As shown in the FT-IR spectra (Fig. 4d), there was a broad band around 800–1500 cm^{-1}, and a new peak was observed at 1080 cm^{-1} for PABC-700. This band is caused by the symmetric vibration of ionized link P–O in P–phosphate ester and the symmetrical vibration of the polyphosphate chain P–O–P (Zeng et al. 2021).

Based on the above characterizations, the mechanism for the construction of micropore dominated functional biochar was speculated as follows: the lignin is the main component of coffee residue (Jeguirim et al. 2014), and high temperature is helpful for the cross-linking of aromatic ring structure and the change of internal microcrystalline structure of lignin, which reduces the degree of graphitization (in accordance with the XRD analysis as shown in Fig. 2a). Activation of phosphoric acid can catalyze the fracture of the functional groups of lignin side chains and their monomers (Xie et al. 2019). At the same time, phosphate derivatives (pyrophosphoric acid and metaphosphoric acid) embedded in lignin structure acted as cross-linking agent of the aromatic ring lamellae of lignin through phosphate ester bond. Thus, the pore structure collapsed due to the thermal shrinkage of aromatic ring condensation at high temperature can be restored and prone to promote the micropore transformation (Pu et al. 2020).

3.2 Adsorption study

As presented in Fig. 5a, c, the initial adsorption rate (h) of PABCs was remarkably accelerated compared with that of ABCs, and PABCs reached adsorption equilibrium within 180 min, while it was 720 min for ABCs. The obtained results analyzed by pseudo-second-order model were shown in Table 2. Pseudo-second-order model resulted in high fit

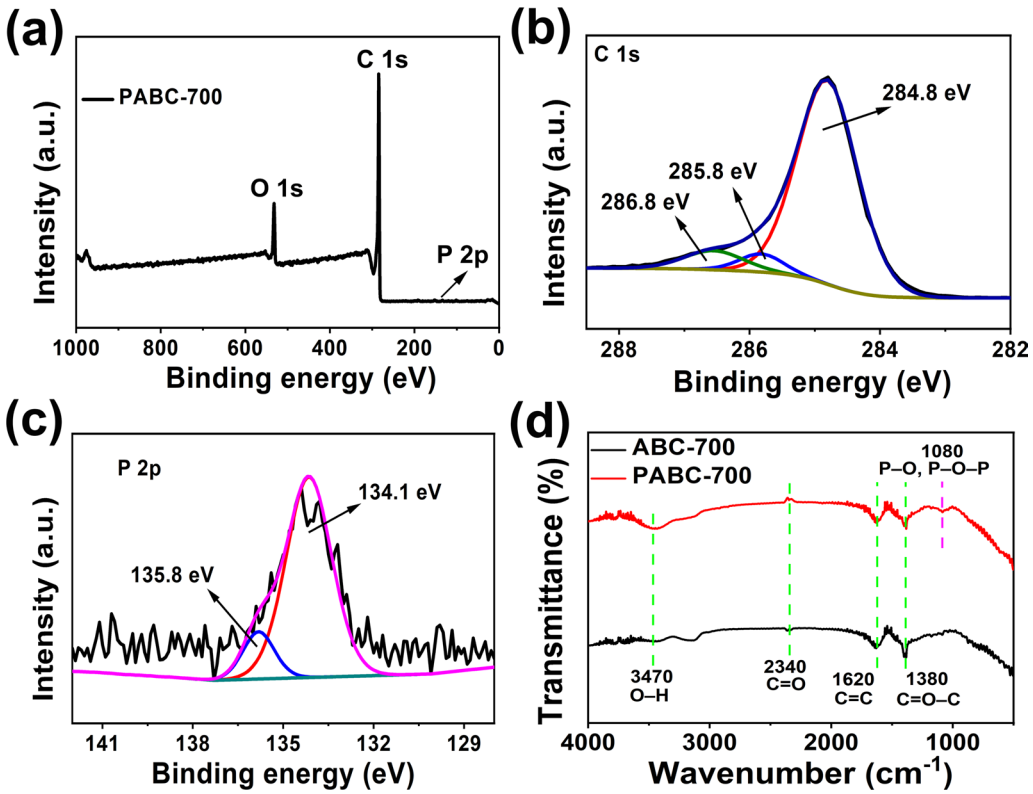

Fig. 4 XPS survey spectra of **a** PABC-700; **b** C1s spectra of PABC-700; **c** P2p spectra of PABC-700; and **d** FTIR spectra of ABC-700 and PABC-700

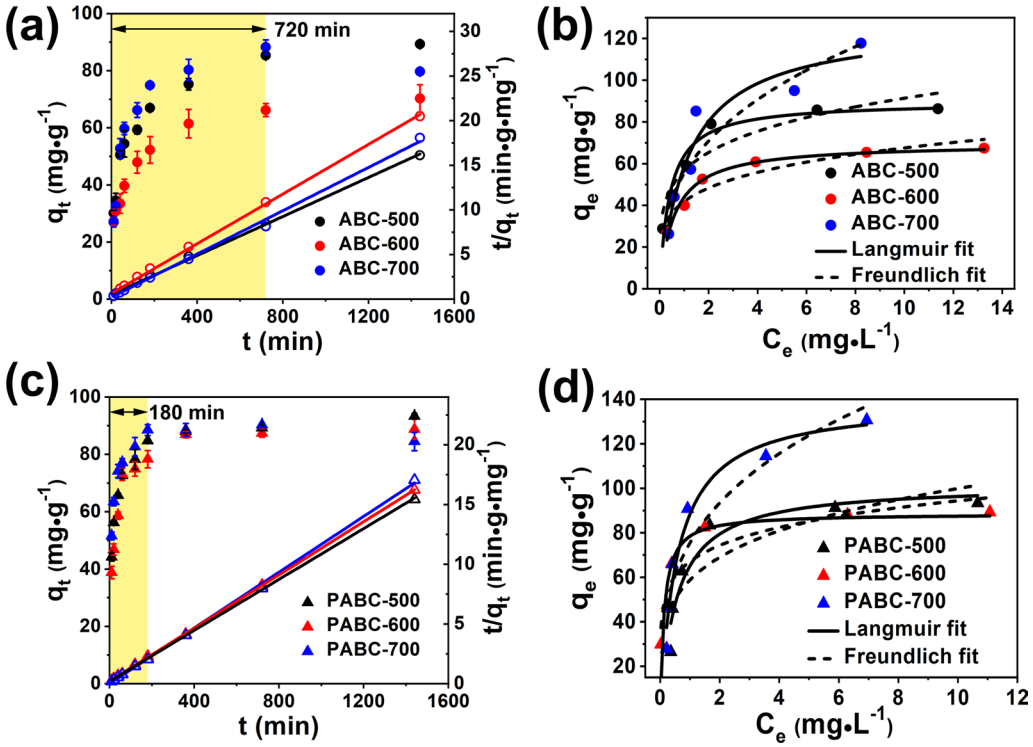

Fig. 5 The SDZ adsorption kinetics and linear fitting plots of **a** ABCs and **c** PABCs; and adsorption isotherm fittings of **b** ABCs and **d** PABCs

Table 2 The pseudo-second-order kinetic curve fitting parameters and adsorption isotherm parameters of ABCs and PABCs

Sample	Pseudo-second-order					Langmuir		Freundich
	q_e (mg/g)	k_2 (L/mg)	h (mg/(g min))	$t_{1/2}$ (min)	R^2	q_m (mg/g)	R^2	R^2
ABC-500	91.4	2.35×10^{-4}	1.96	46.6	0.998	98.1	0.951	0.864
ABC-600	71.8	2.99×10^{-4}	1.54	46.6	0.998	69.6	0.975	0.912
ABC-700	82.5	6.96×10^{-4}	4.74	17.4	0.996	127.2	0.907	0.857
PABC-500	93.8	5.54×10^{-4}	4.88	19.2	0.999	101.7	0.909	0.716
PABC-600	89.8	5.96×10^{-4}	4.81	18.7	0.999	88.5	0.955	0.886
PABC-700	91.4	1.16×10^{-3}	9.66	9.46	0.999	139.2	0.963	0.869

degree for all biochars, and attested that the adsorption process was mainly controlled by chemical process rather than the mass transfer step (Liu et al. 2020b). According to the pseudo-second-order kinetic fitting parameters, the equilibrium adsorption capacity (q_e) of PABCs was about 10% higher than that of ABCs. Significantly, the adsorption rate constant (k_2) and initial adsorption rate (h) of PABCs were about twicethose of ABCs, and the adsorption half-life ($t_{1/2}$) of PABCs was greatly shortened. The initial adsorption rate of SDZ followed the sequence of PABC-700 > PABC-500 > PABC-600, ABC-700 > ABC-500 > ABC-600. This phenomenon was speculated to be caused by their surface characteristics and specific adsorptive interactions. PABCs possessed excellent porosity (as shown in Table 1), which could provide more adsorption sites.

The adsorption isotherms for SDZ in both ABCs and PABCs are shown in Fig. 5b, d. It was obvious that the data could be better fitting the Langmuir model (Table 2),indicating a monolayer adsorption (Zhou et al. 2017). The maximum adsorption capacities (q_m) of biochar to sulfadiazine followed the order of PABC-700 > PABC-500 > PABC-600, ABC-700 > ABC-500 > ABC-600.

3.3 Comparisons of the sulfadiazine adsorption performance

The adsorption performance of various adsorbents for SDZ was compared (Table 3). The adsorption capacity of PABC-700 prepared in this work was 46–80% higher than that of the reported activated biochars (He et al. 2021; Zhang et al. 2021a; Wang et al. 2019; Meng et al. 2020), exceeding that

Table 3 The adsorption capacity of sulfadiazine with various adsorbents

Absorbent	Specific surface area (m^2/g)	Adsorbent dosage (g/L)	q_m (mg/g)	K_L (L/mg)	References
Stalk cellulose	1.83	–	1.385	1.248	Zheng et al. (2020)
Corn straw biochar	19.6	1	2.640	0.263	Zhang et al. (2021b)
Graphene oxide	–	0.25	6.27	7.21	Zhong et al. (2020)
Tea waste biochar	717.636	0.5	77.52	3.15	He et al. (2021)
Maize straw biochar	1065	0.125	86.5	1.03	Zhang et al. (2021a)
Coffee grounds-based biochar	1707	0.1	90.7	7.10	Wang et al. (2019)
Cotton shell biochar	1225.6	1	95.24	0.40	Meng et al. (2020)
Multi-walled carbon nanotubes	–	1	132.334	0.172	Liu et al. (2020c)
Commercially activated carbon	745.4	0.1	137.22	0.73	Berges et al. (2021)
Boron nitride bundles	871.456	0.2	137.728	0.305	Song et al. (2019)
PABC-700	1365	0.1	139.2	1.74	This work

of carbon nanotubes (Liu et al. 2020c) and commercially available activated carbon (Berges et al. 2021). Besides, PABC-700 demonstrated higher adsorption affinity (as indicated from K_L) compared to other adsorbents with similar adsorption capacity. And the K_L of PABC-700 was even 10 times that of multi-walled carbon nanotubes (Liu et al. 2020c). It was of great importance to find that the phosphoric acid modified coffee grounds-based biochar had both high adsorption capacity and adsorption affinity.

The large adsorption capacity and affinity should be ascribed to the micropore structure of the PABC-700 and the physicochemical properties of biochars and antibiotics. The contact angles (CA) were determined and the results are shown in Fig. S3. The improvement of surface hydrophobicity after phosphoric acid modification was confirmed lying on the fact that the CA values of PABC-500, PABC-600 and PABC-700 were raised to 138.8°, 139.9° and 141.7°, respectively. The hydrophobic amide structure of sulfadiazine would have great affinity with the hydrophobic groups on the surface of biochar through hydrophobic partition (Ovung and Bhattacharyya 2021). In addition, as the micropores represented almost 85% of the pore volume, the hydrophobic cavities of these micropores exhibited a confinement effects for the adsorption of SDZ (Luo et al. 2020) to illustrate an accelerated initial adsorption rate. The I_D/I_G of PABC-700 further dropped to 1.290 after use (as shown in Fig. 2b), indicating more defect sites were taken by the adsorbents. Furthermore, the gathering of the surface functional groups played a crucial role in the adsorption process. In particular, phosphorus-containing functional groups were successfully introduced to the PABC-700 surface through phosphoric acid modification (as shown in Fig. 4d), which allowed the adsorbent to bind to the surface of the adsorbent faster (Ahmed et al. 2017). On one hand, SDZ molecules acted as π–electron acceptors due totheir amino functional groups. On the other hand, the biochar surface was rich in C=C, C–O, and –OH functional groups (as shown in Fig. 4d) to demonstrate a strong ability to donate electrons. In addition, biochars prepared at high temperatures possessed high content of electron rich aromatic rings, which presented strong electron donating ability to form the cation–π interaction with SDZ (Ahmed et al. 2017; Peiris et al. 2017). Therefore, the surface hydrophobicity together with the π–π electron–donor–acceptor (EDA) interaction was speculated to play the leading role for binding SDZ (Teixido et al. 2011; Zhang et al. 2016).

3.4 Effect of pH

The points of zero charge (pH_{PZC}) of ABC-700 and PABC-700 were then determined to explain the surface charge alteration at a wide pH range as shown in Fig. 6. The results showed that the pH_{PZC} for ABC-700 and PABC-700 were 4.5 and 1.2, respectively. The acidic migration for isoelectric point of PABC-700 was ascribed to the abundant acidic functional groups on the biochar surface after H_3PO_4 modification. Moreover, according to the dissociation constants

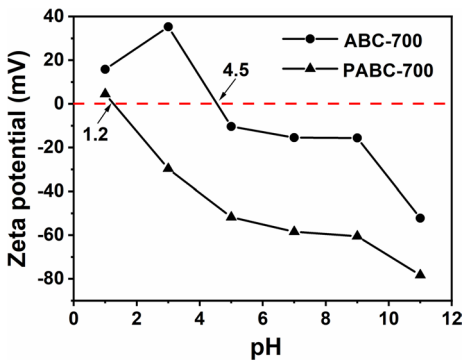

Fig. 6 The Zeta potential plots of ABC-700 and PABC-700

of SDZ, when pH < 1.57, most of SDZ existed in the form of cations (SDZ^+) (Yang et al. 2019b), which supported the phenomenon that modified biochars were more favorable for the adsorption of SDZ at low pH driven by electrostatic forces (Table 4). Contrarily, when pH > 6.5, SDZ mostly existed in the form of anions (SDZ^-), at which the negative surface zeta potential value of biochars resulted in electrostatic repulsion with the SDZ molecule, causing a decrease of equilibrium adsorption capacity (q_e) and initial adsorption rates (h) as shown in Fig. 7c, d.

As pH had significant effects on the existing forms of SDZ as well as the functional groups located on biochars, its influence on SDZ adsorption process was investigated. At low pH, the protonated amino groups ($–NH_3^+$) on sulfadiazine and the hydroxyl group on the biochars formed strong EDA interaction. The amino groups ($–NH_2$) of sulfadiazine were presented as protonated amino groups ($–NH_3^+$) at low pH. Hence, hydrogen bonding was likely to exist between the $–NH_3^+$ groups in SDZ and the oxygenated groups on the surface of PABCs (Chen et al. 2019; Wang et al. 2020). Sulfadiazine behaved as neutral species that consisted of sulfonamide groups and lone pair electron rich N atoms when the pH valueranged from 1.57 to 6.5. Thus, Lewis acid–base interactions could contribute to the adsorption affinities due to the extra interaction between the lone pair electron on the SDZ and protons from carboxylic and hydroxyl groups on the PABCs surface (Yang et al. 2019b). As pH increased to 7 and 9, the surface of ABC-700 and PABC-700 became negatively charged while sulfadiazine also existed in negative species [> pKa_2 (6.5)]. Within this range, ABC-700 and PABC-700 maintained good q_e even though the electrostatic repulsion emerged. This was an indication as π–π electron–donor–acceptor (EDA) interaction and surface hydrophobicity still played the leading role. However, at

Table 4 The pseudo-second-order kinetic curve fitting parameters of ABC-700 and PABC-700 at different pH

pH	ABC-700				PABC-700			
	q_e (mg/g)	h (mg/(g min))	$t_{1/2}$ (min)	R^2	q_e (mg/g)	h (mg/(g min))	$t_{1/2}$ (min)	R^2
3	98.3	5.08	19.4	0.999	97.2	19.92	4.9	0.999
5	99.0	6.57	15.1	0.999	98.5	15.54	6.3	0.999
7	97.1	4.36	22.3	0.999	97.9	7.22	13.6	0.999
9	82.5	4.74	17.4	0.999	91.4	9.66	9.4	0.999
11	45.5	0.94	48.5	0.999	37.3	0.96	38.9	0.999

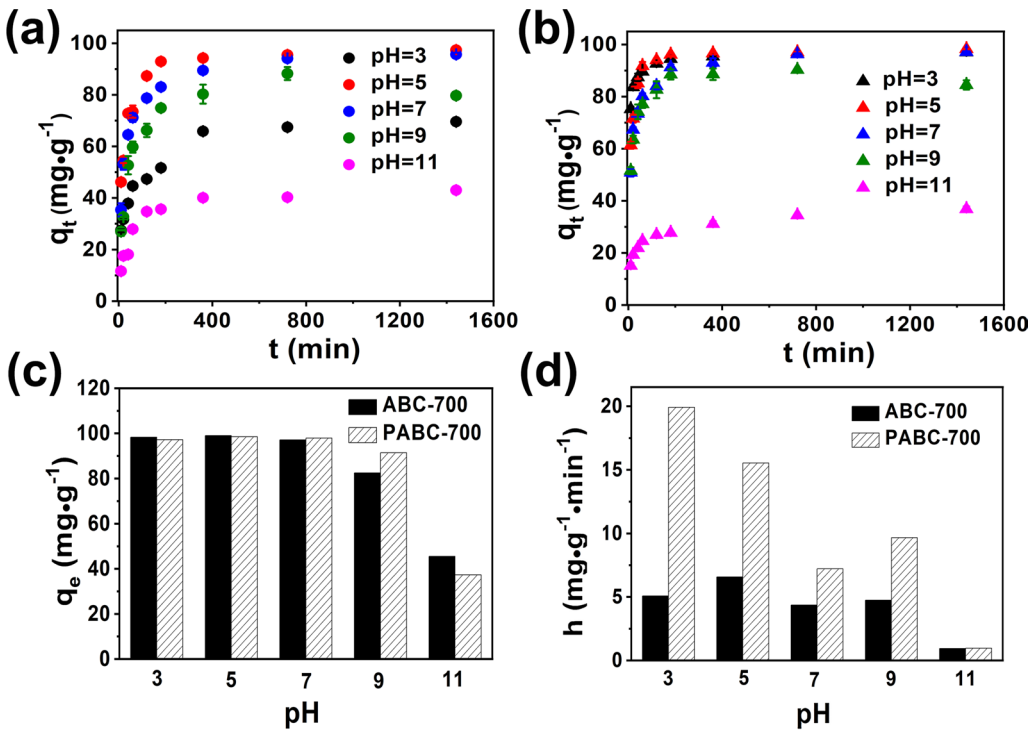

Fig. 7 The SDZ adsorption kineticsof **a** ABC-700 and **b** PABC-700; and the comparison of **c** q_e and **d** h of both materials at pH of 3.0–11.0

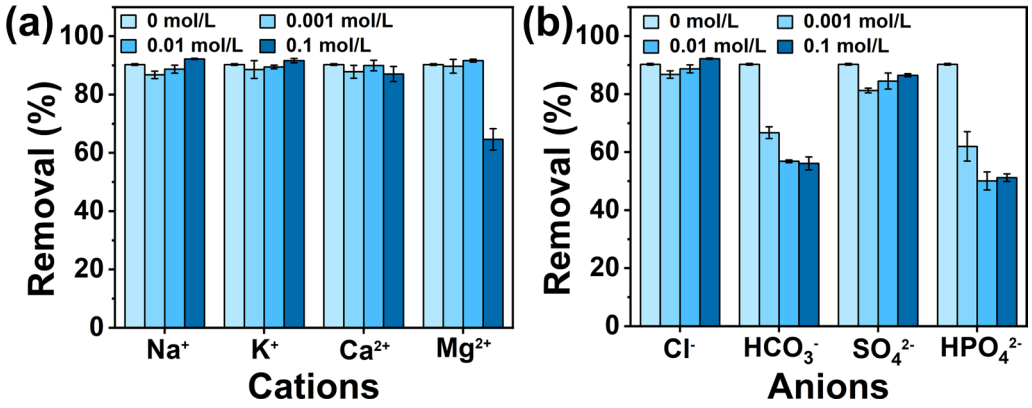

Fig. 8 Added cations (Na^+, K^+, Ca^{2+}, Mg^{2+}using NaCl, KCl, $CaCl_2$ and $MgCl_2$, respectively) (**a**) and added anions (Cl^-, HCO_3^-, SO_4^{2-}, HPO_4^{2-}, using NaCl, $NaHCO_3$, Na_2SO_4 and Na_2HPO_4, respectively) (**b**) affecting SDZ adsorption on PABC-700

pH up to 11.0, the adsorption of sulfadiazine by ABCs and PABCs significantly decreased due to the strong electrostatic repulsion between SDZ^- species and the negative surface of ABCs and PABCs.

3.5 Effect of ionic strength, cations and anions on sorption

The impacts of coexisting ions in water on the adsorption effects of SDZ were fully revealed according to the results obtained from the systematical examinations of the cationic and anionic species, valences, and concentrations (as shown in Fig. 8). The SDZ removal efficiency was slightly improved with respect to the addition of monovalent cations, such as Na^+ and K^+. This could be explained with the salting-out effects which lead to the hydrophobic SDZ less dissolved in water while adsorbed more on the PABC surfaces. However, this phenomenon did not simply occur when divalent cations, such as Ca^{2+} and Mg^{2+} were under consideration. Interestingly, there was a game relationship between the salting-out and squeezing-out effects (Zhang et al. 2010). In other words, the salting-out effect dominated for cations at low concentrations and thus caused the improvement in the removal efficiency. Nevertheless, the squeezing-out effects, inducing the compacting of porous structures, which was against for SDZ adsorption, would play the leading role in keeping lifting the concentrations, and inhibiting the adsorption efficiency thereafter (Jiang et al. 2016). Adding Cl^- or SO_4^{2-} had negligible effect on SDZ sorption (Fig. 8b). However, HCO_3^- and HPO_4^{2-} had negative impact on SDZ removal. The aqueous solutions of $NaHCO_3$ and $NaHPO_4$ were weakly alkaline, and the electrostatic repulsion between SDZ^- species and the negative surface of PABC-700 under alkaline conditions was the main reason for the decrease of removal efficiency.

4 Conclusions

The micropore dominated activated carbons with remarkably high adsorption capacity and affinity for SDZ were prepared via alkali/phosphoric acid modification using carbonized coffee grounds. The maximum adsorption capacity of biochars followed the order of PABC-700 > PABC-500 > PABC-600, ABC-700 > ABC-500 > ABC-600. The results demonstrated that phosphoric acid modification and pyrolysis temperatures had significant effects on the properties of the PABCs, and consequently PABC-700 showed optimal SDZ adsorption capacity. In particular, the adsorption affinity was greatly improved to be competitive to the latest boron nitride bundles and multi-walled carbon nanotubes. It is believed that excellent porosity, newly formed phosphate, enriched acidic and carboxyl groups made a significant contribution for increasing the q_m of PABC-700. In addition, the effects of temperature should be emphasized during the preparation process of biochar to avoid the blocking of porous structures by tars and volatiles generated during pyrolysis. Overall, this study provides an efficient sulfadiazine removal technology, as well as supplies an economical and environmentally friendly approach for coffee grounds disposal.

Supplementary Information The online version contains supplementary material available at https://doi.org/10.1007/s42773-022-00143-4.

Acknowledgements We are grateful for financial support from the Key Laboratory of Functional Inorganic Material Chemistry (Heilongjiang University), Ministry of Education, Project of Fujian Provincial Department of Science and Technology (2021J01121), the Fujian Agriculture and Forestry University Program for Distinguished Young Scholar (Grant No. xjq201813), the Open Project Program of the State Key Laboratory of Photocatalysis on Energy and Environment (Grant

No. SKLPEE-202008), Fuzhou University, and the Special Fund for Scientific and Technological Innovation of Fujian Agriculture and Forestry University (Grant No. CXZX2019073G).

Author contributions XYZ performed the experimental work about PABCs, data analysis and drafted the manuscript. YW performed the adsorption using PABCs. RXL performed the adsorption experimental work about ABCs. The project was conceived, planned, and supervised by HLC, YFL, and JL. All authors discussed the results. The author read and approved the final manuscript.

Funding This work was funded by the Key Laboratory of Functional Inorganic Material Chemistry (Heilongjiang University), Ministry of Education, Project of Fujian Provincial Department of Science and Technology (2021J01121), the Fujian Agriculture and Forestry University Program for Distinguished Young Scholar (Grant No. xjq201813), the Open Project Program of the State Key Laboratory of Photocatalysis on Energy and Environment (Grant No. SKLPEE-202008), Fuzhou University, and the Special Fund for Scientific and Technological Innovation of Fujian Agriculture and Forestry University (Grant No. CXZX2019073G).

Availability of data and materials All data generated or analysed during this study are included in this article.

Declarations

Conflict of interests The authors declare that they have no known competing financial interests or personal relationships that could have appeared to influence the work reported in this paper.

References

Ahmed MB, Zhou JL, Ngo HH, Guo WS, Johir MA, Sornalingam K (2017) Single and competitive sorption properties and mechanism of functionalized biochar for removing sulfonamide antibiotics from water. Chem Eng J 311:348–358. https://doi.org/10.1016/j.cej.2016.11.106

Angin D, Sensoz S (2014) Effect of pyrolysis temperature on chemical and surface properties of biochar of rapeseed. Int J Phytoremediat 16:684–693. https://doi.org/10.1080/15226514.2013.856842

Angin D, Altintig E, Kose TE (2013) Influence of process parameters on the surface and chemical properties of activated carbon obtained from biochar by chemical activation. Bioresour Technol 148:542–549. https://doi.org/10.1016/j.biortech.2013.08.164

Antonangelo JA, Zhang HL, Sun X, Kumar A (2019) Physicochemical properties and morphology of biochars as affected by feedstock sources and pyrolysis temperatures. Biochar 1:325–336. https://doi.org/10.1007/s42773-019-00028-z

Bai YW, Meng W, Xu J, Zhang Y, Guo CS (2014) Occurrence, distribution and bioaccumulation of antibiotics in the Liao River Basin in China. Environ Sci-Proc Impacts 16:586–593. https://doi.org/10.1039/c3em00567d

Bashir S, Zhu J, Fu QL, Hu HQ (2018) Comparing the adsorption mechanism of Cd by rice straw pristine and KOH-modified biochar. Environ Sci Pollut Res 25:11875–11883. https://doi.org/10.1007/s11356-018-1292-z

Berges J, Moles S, Ormad MP, Mosteo R, Gomez J (2021) Antibiotics removal from aquatic environments: adsorption of enrofloxacin, trimethoprim, sulfadiazine, and amoxicillin on vegetal powdered activated carbon. Environ Sci Pollut Res 28:8442–8452. https://doi.org/10.1007/s11356-020-10972-0

Bougnom BP, Piddock LJV (2017) Wastewater for urban agriculture: a significant factor in dissemination of antibiotic resistance. Environ Sci Technol 51:5863–5864. https://doi.org/10.1021/acs.est.7b01852

Chen T, Luo L, Deng S, Shi G, Zhang S, Zhang Y, Deng O, Wang L, Zhang J, Wei L (2018) Sorption of tetracycline on H_3PO_4 modified biochar derived from rice straw and swine manure. Bioresour Technol 267:431–437. https://doi.org/10.1016/j.biortech.2018.07.074

Chen Z, Xiao X, Xing B, Chen B (2019) pH-dependent sorption of sulfonamide antibiotics onto biochars: sorption mechanisms and modeling. Environ Pollut 248:48–56. https://doi.org/10.1016/j.envpol.2019.01.087

Choi YK, Kan E (2019) Effects of pyrolysis temperature on the physicochemical properties of alfalfa-derived biochar for the adsorption of bisphenol A and sulfamethoxazole in water. Chemosphere 218:741–748. https://doi.org/10.1016/j.chemosphere.2018.11.151

Chu G, Zhao J, Huang Y, Zhou D, Liu Y, Wu M, Peng H, Zhao Q, Pan B, Steinberg CEW (2018) Phosphoric acid pretreatment enhances the specific surface areas of biochars by generation of micropores. Environ Pollut 240:1–9. https://doi.org/10.1016/j.envpol.2018.04.003

Dai J, Meng X, Zhang Y, Huang Y (2020) Effects of modification and magnetization of rice straw derived biochar on adsorption of tetracycline from water. Bioresour Technol 311:123455. https://doi.org/10.1016/j.biortech.2020.123455

Davies J, Davies D (2010) Origins and evolution of antibiotic resistance. Microbiol Mol Biol Rev 74:417–433. https://doi.org/10.1128/mmbr.00016-10

Deng J, Xiong TY, Xu F, Li MM, Han CL, Gong YT, Wang HY, Wang Y (2015) Inspired by bread leavening: one-pot synthesis of hierarchically porous carbon for supercapacitors. Green Chem 17:4053–4060. https://doi.org/10.1039/c5gc00523j

Gao Y, Li Y, Zhang L, Huang H, Hu J, Shah SM, Su X (2012) Adsorption and removal of tetracycline antibiotics from aqueous solution by graphene oxide. J Colloid Interface Sci 368:540–546. https://doi.org/10.1016/j.jcis.2011.11.015

Gao L, Li ZH, Yi WM, Li YF, Zhang P, Zhang AD, Wang LH (2021) Impacts of pyrolysis temperature on lead adsorption by cotton stalk-derived biochar and related mechanisms. J Environ Chem Eng 9:105602. https://doi.org/10.1016/j.jece.2021.105602

Guo ZZ, Zhang J, Kang Y, Liu H (2017) Rapid and efficient removal of Pb(II) from aqueous solutions using biomass-derived activated carbon with humic acid in-situ modification. Ecotoxicol Environ Saf 145:442–448. https://doi.org/10.1016/j.ecoenv.2017.07.061

He XL, Li JL, Meng QM, Guo ZY, Zhang H, Liu YR (2021) Enhanced adsorption capacity of sulfadiazine on tea waste biochar from aqueous solutions by the two-step sintering method without corrosive activator. J Environ Chem Eng 9:104898. https://doi.org/10.1016/j.jece.2020.104898

Ho YS (2006) Review of second-order models for adsorption systems. J Hazard Mater 136:681–689. https://doi.org/10.1016/j.jhazmat.2005.12.043

Hopkins D, Hawboldt K (2020) Biochar for the removal of metals from solution: a review of lignocellulosic and novel marine feedstocks. J Environ Chem Eng 8:103975. https://doi.org/10.1016/j.jece.2020.103975

Hu B, Ai Y, Jin J, Hayat T, Alsaedi A, Zhuang L, Wang X (2020) Efficient elimination of organic and inorganic pollutants by biochar and biochar-based materials. Biochar 2:47–64. https://doi.org/10.1007/s42773-020-00044-4

Huff MD, Lee JW (2016) Biochar-surface oxygenation with hydrogen peroxide. J Environ Manag 165:17–21. https://doi.org/10.1016/j.jenvman.2015.08.046

Jeguirim M, Limousy L, Dutournie P (2014) Pyrolysis kinetics and physicochemical properties of agropellets produced from spent ground coffee blended with conventional biomass. Chem Eng Res Des 92:1876–1882. https://doi.org/10.1016/j.cherd.2014.04.018

Jiang LH, Liu YG, Zeng GM, Xiao FY, Hu XJ, Hu X, Wang H, Li TT, Zhou L, Tan XF (2016) Removal of 17 beta-estradiol by few-layered graphene oxide nanosheets from aqueous solutions: external influence and adsorption mechanism. Chem Eng J 284:93–102. https://doi.org/10.1016/j.cej.2015.08.139

Kang C, Zhu L, Wang Y, Wang Y, Xiao K, Tian T (2018) Adsorption of basic dyes using walnut shell-based biochar produced by hydrothermal carbonization. Chem Res Chin Univ 34:622–627. https://doi.org/10.1007/s40242-018-8018-0

Kim HY, Jeon J, Hollender J, Yu S, Kim SD (2014) Aqueous and dietary bioaccumulation of antibiotic tetracycline in *D. magna* and its multigenerational transfer. J Hazard Mater 279:428–435. https://doi.org/10.1016/j.jhazmat.2014.07.031

Kim JE, Bhatia SK, Song HJ, Yoo E, Jeon HJ, Yoon JY, Yang Y, Gurav R, Yang YH, Kim HJ, Choi YK (2020) Adsorptive removal of tetracycline from aqueous solution by maple leaf-derived biochar. Bioresour Technol 306:123092. https://doi.org/10.1016/j.biortech.2020.123092

Kummerer K (2002) Drugs in the environment: emission of drugs, diagnostic aids and disinfectants into wastewater by hospitals in relation to other sources—a review. Chemosphere 48:383–383. https://doi.org/10.1016/S0045-6535(02)00088-7

Lange R, Dietrich D (2002) Environmental risk assessment of pharmaceutical drug substances—conceptual considerations. Toxicol Lett 131:97–104. https://doi.org/10.1016/S0378-4274(02)00071-1

Li WW, Amin FR, Fu YS, Zhang H, He YF, Huang Y, Liu GQ, Chen C (2019) Effects of temperature, heating rate, residence time, reaction atmosphere, and pressure on biochar properties. J Biobased Mater Bioenergy 13:1–10. https://doi.org/10.1166/jbmb.2019.1789

Ling C, Li X, Zhang Z, Liu F, Deng Y, Zhang X, Li A, He L, Xing B (2016) High adsorption of sulfamethoxazole by an amine-modified polystyrene-divinylbenzene resin and its mechanistic insight. Environ Sci Technol 50:10015–10023. https://doi.org/10.1021/acs.est.6b02846

Liu H, Zhang J, Bao N, Cheng C, Ren L, Zhang CL (2012) Textural properties and surface chemistry of lotus stalk-derived activated carbons prepared using different phosphorus oxyacids: adsorption of trimethoprim. J Hazard Mater 235:367–375. https://doi.org/10.1016/j.jhazmat.2012.08.015

Liu WJ, Li WW, Jiang H, Yu HQ (2017) Fates of chemical elements in biomass during its pyrolysis. Chem Rev 117:6367–6398. https://doi.org/10.1021/acs.chemrev.6b00647

Liu C, Wang W, Wu R, Liu Y, Lin X, Kan H, Zheng Y (2020a) Preparation of acid- and alkali-modified biochar for removal of methylene blue pigment. ACS Omega 5:30906–30922. https://doi.org/10.1021/acsomega.0c03688=

Liu LQ, Deng GZ, Shi XY (2020b) Adsorption characteristics and mechanism of p-nitrophenol by pine sawdust biochar samples produced at different pyrolysis temperatures. Sci Rep 10:5149. https://doi.org/10.1038/s41598-020-62059-y

Liu YB, Peng YL, An BH, Li LC, Liu Y (2020c) Effect of molecular structure on the adsorption affinity of sulfonamides onto CNTs: batch experiments and DFT calculations. Chemosphere 246:125778. https://doi.org/10.1016/j.chemosphere.2019.125778

Luo T, Shakya S, Mittal P, Ren XH, Guo T, Bello MG, Wu L, Li HY, Zhu WF, Regmi B, Zhang JW (2020) Co-delivery of superfine nano-silver and solubilized sulfadiazine for enhanced antibacterial functions. Int J Pharm 584:119407. https://doi.org/10.1016/j.ijpharm.2020.119407

Ma ZQ, Chen DY, Gu J, Bao BF, Zhang QS (2015) Determination of pyrolysis characteristics and kinetics of palm kernel shell using TGA-FTIR and model-free integral methods. Energy Convers Manag 89:251–259. https://doi.org/10.1016/j.enconman.2014.09.074

Martucci A, Braschi I, Marchese L, Quartieri S (2014) Recent advances in clean-up strategies of waters polluted with sulfonamide antibiotics: a review of sorbents and related properties. Mineral Mag 78:1115–1140. https://doi.org/10.1180/minmag.2014.078.5.03

Meng QM, Zhang YL, Meng D, Liu XP, Zhang ZJ, Gao PL, Lin AG, Hou L (2020) Removal of sulfadiazine from aqueous solution by in-situ activated biochar derived from cotton shell. Environ Res 191:110104. https://doi.org/10.1016/j.envres.2020.110104

Nakata H, Kannan K, Jones PD, Giesy JP (2005) Determination of fluoroquinolone antibiotics in wastewater effluents by liquid chromatography–mass spectrometry and fluorescence detection. Chemosphere 58:759–766. https://doi.org/10.1016/j.chemosphere.2004.08.097

Ndoun MC, Elliott HA, Preisendanz HE, Williams CF, Knopf A, Watson JE (2020) Adsorption of pharmaceuticals from aqueous solutions using biochar derived from cotton gin waste and guayule bagasse. Biochar 3:89–104. https://doi.org/10.1007/s42773-020-00070-2

Oginni O, Yakaboylu GA, Singh K, Sabolsky EM, Unal-Tosun G, Jaisi D, Khanal S, Shah A (2020) Phosphorus adsorption behaviors of MgO modified biochars derived from waste woody biomass resources. J Environ Chem Eng 8:103723. https://doi.org/10.1016/j.jece.2020.103723

Ovung A, Bhattacharyya J (2021) Sulfonamide drugs: structure, antibacterial property, toxicity, and biophysical interactions. Biophys Rev 13:259–272. https://doi.org/10.1007/s12551-021-00795-9

Pan N, Tang J, Hou DZ, Lei H, Zhou DH, Ding J (2021) Enhanced uranium uptake from acidic media achieved on a novel iron phosphate adsorbent. Chem Eng J 423:130267. https://doi.org/10.1016/j.cej.2021.130267

Peiris C, Gunatilake SR, Mlsna TE, Mohan D, Vithanage M (2017) Biochar based removal of antibiotic sulfonamides and tetracyclines in aquatic environments: a critical review. Bioresour Technol 246:150–159. https://doi.org/10.1016/j.biortech.2017.07.150

Peng HB, Gao P, Chu G, Pan B, Peng JH, Xing BS (2017) Enhanced adsorption of Cu(II) and Cd(II) by phosphoric acid-modified biochars. Environ Pollut 229:846–853. https://doi.org/10.1016/j.envpol.2017.07.004

Poloni V, Salvato L, Pereyra C, Oliveira A, Rosa C, Cavaglieri L, Keller KM (2017) Bakery by-products based feeds borne-*Saccharomyces cerevisiae* strains with probiotic and antimycotoxin effects plus antibiotic resistance properties for use in animal production. Food Chem Toxicol 107:630–636. https://doi.org/10.1016/j.fct.2017.02.040

Prahas D, Kartika Y, Indraswati N, Ismadji S (2008) Activated carbon from jackfruit peel waste by H_3PO_4 chemical activation: pore structure and surface chemistry characterization. Chem Eng J 140:32–42. https://doi.org/10.1016/j.cej.2007.08.032

Pu Y, Xu S, Wang K, Feng Y, Wang W (2020) Study on the activation process of lignin based activated carbon by phosphoric acid method. J Dalian Univ Technol 60:350–357. https://doi.org/10.7511/d11gxb202004003

Quah RV, Tan YH, Mubarak NM, Kansedo J, Khalid M, Abdullah EC, Abdullah MO (2020) Magnetic biochar derived from waste palm kernel shell for biodiesel production via sulfonation. Waste Manag 118:626–636. https://doi.org/10.1016/j.wasman.2020.09.016

Reza MS, Afroze S, Bakar MSA, Saidur R, Aslfattahi N, Taweekun J, Azad AK (2020) Biochar characterization of invasive *Pennisetum purpureum* grass: effect of pyrolysis temperature. Biochar 2:239–251. https://doi.org/10.1007/s42773-020-00048-0

Sakhiya AK, Anand A, Kaushal P (2020) Production, activation, and applications of biochar in recent times. Biochar 2:253–285. https://doi.org/10.1007/s42773-020-00047-1

Song QQ, Liang JL, Fang Y, Cao CC, Liu ZY, Li LL, Huang Y, Lin J, Tang CC (2019) Selective adsorption behavior/mechanism of antibiotic contaminants on novel boron nitride bundles. J Hazard Mater 364:654–662. https://doi.org/10.1016/j.jhazmat.2018.10.054

Suliman W, Harsh JB, Abu-Lail NI, Fortuna AM, Dallmeyer I, Garcia-Perez M (2016) Modification of biochar surface by air oxidation: role of pyrolysis temperature. Biomass Bioenergy 85:1–11. https://doi.org/10.1016/j.biombioe.2015.11.030

Tan XF, Liu YG, Zeng GM, Wang X, Hu XJ, Gu YL, Yang ZZ (2015) Application of biochar for the removal of pollutants from aqueous solutions. Chemosphere 125:70–85. https://doi.org/10.1016/j.chemosphere.2014.12.058

Tang L, Yu JF, Pang Y, Zeng GM, Deng YC, Wang JJ, Ren XY, Ye SJ, Peng B, Feng HP (2018) Sustainable efficient adsorbent: alkali-acid modified magnetic biochar derived from sewage sludge for aqueous organic contaminant removal. Chem Eng J 336:160–169. https://doi.org/10.1016/j.cej.2017.11.048

Teixido M, Pignatello JJ, Beltran JL, Granados M, Peccia J (2011) Speciation of the ionizable antibiotic sulfamethazine on black carbon (biochar). Environ Sci Technol 45:10020–10027. https://doi.org/10.1021/es202487h

Tomczyk A, Sokolowska Z, Boguta P (2020) Biochar physicochemical properties: pyrolysis temperature and feedstock kind effects. Rev Environ Sci Bio/Technol 19:191–215. https://doi.org/10.1007/s11157-020-09523-3

Tripathi M, Sahu JN, Ganesan P (2016) Effect of process parameters on production of biochar from biomass waste through pyrolysis: a review. Renew Sustain Energy Rev 55:467–481. https://doi.org/10.1016/j.rser.2015.10.122

Vardon DR, Moser BR, Zheng W, Witkin K, Evangelista RL, Strathmann TJ, Rajagopalan K, Sharma BK (2013) Complete utilization of spent coffee grounds to produce biodiesel, bio-oil, and biochar. Acs Sustain Chem Eng 1:1286–1294. https://doi.org/10.1021/sc400145w

Vithanage M, Rajapaksha AU, Zhang M, Thiele-Bruhn S, Lee SS, Ok YS (2015) Acid-activated biochar increased sulfamethazine retention in soils. Environ Sci Pollut Res 22:2175–2186. https://doi.org/10.1007/s11356-014-3434-2

Wang JC, Kaskel S (2012) KOH activation of carbon-based materials for energy storage. J Mater Chem 22:23710–23725. https://doi.org/10.1039/c2jm34066f

Wang JL, Wang SZ (2019) Preparation, modification and environmental application of biochar: a review. J Clean Prod 227:1002–1022. https://doi.org/10.1016/j.jclepro.2019.04.282

Wang Y, Jiao WB, Wang JT, Liu GF, Cao HL, Lu J (2019) Amino-functionalized biomass-derived porous carbons with enhanced aqueous adsorption affinity and sensitivity of sulfonamide antibiotics. Bioresour Technol 277:128–135. https://doi.org/10.1016/j.biortech.2019.01.033

Wang B, Xu X, Tang H, Mao Y, Chen H, Ji F (2020) Highly efficient adsorption of three antibiotics from aqueous solutions using glucose-based mesoporous carbon. Appl Surf Sci. https://doi.org/10.1016/j.apsusc.2020.147048

Wei JM, Sun WL, Pan WY, Yu XQ, Sun G, Jiang H (2017) Comparing the effects of different oxygen-containing functional groups on sulfonamides adsorption by carbon nanotubes: experiments and theoretical calculation. Chem Eng J 312:167–179. https://doi.org/10.1016/j.cej.2016.11.133

Xiao X, Chen ZM, Chen BL (2016) H/C atomic ratio as a smart linkage between pyrolytic temperatures, aromatic clusters and sorption properties of biochars derived from diverse precursory materials. Sci Rep 6:22644. https://doi.org/10.1038/srep22644

Xiao X, Chen BL, Chen ZM, Zhu LZ, Schnoor JL (2018) Insight into multiple and multilevel structures of biochars and their potential environmental applications: a critical review. Environ Sci Technol 52:5027–5047. https://doi.org/10.1021/acs.est.7b06487

Xie JK, Han QN, Feng B, Liu ZG (2019) Preparation of amphiphilic mesoporous carbon-based solid acid from kraft lignin activated by phosphoric acid and its catalytic performance for hydration of alpha-pinene. Bioresources 14:4284–4303. https://doi.org/10.15376/biores.14.2.4284-4303

Yan MT, Xu C, Huang YM, Nie HY, Wang J (2018) Tetracyclines, sulfonamides and quinolones and their corresponding resistance genes in the Three Gorges Reservoir, China. Sci Total Environ 631–632:840–848. https://doi.org/10.1016/j.scitotenv.2018.03.085

Yang F, Sun L, Zhang W, Zhang Y (2017) One-pot synthesis of porous carbon foam derived from corn straw: atrazine adsorption equilibrium and kinetics. Environ Sci-Nano 4:625–635. https://doi.org/10.1039/c6en00574h

Yang F, Zhang SS, Sun YQ, Du Q, Song JP, Tsang DCW (2019a) A novel electrochemical modification combined with one-step pyrolysis for preparation of sustainable thorn-like iron-based biochar composites. Bioresour Technol 274:379–385. https://doi.org/10.1016/j.biortech.2018.10.042

Yang Y, Zheng L, Zhang T, Yu H, Zhan Y, Yang Y, Zeng H, Chen S, Peng D (2019b) Adsorption behavior and mechanism of sulfonamides on phosphonic chelating cellulose under different pH effects. Bioresour Technol 288:121510. https://doi.org/10.1016/j.biortech.2019.121510

Yao Y, Gao B, Inyang M, Zimmerman AR, Cao XD, Pullammanappallil P, Yang LY (2011) Removal of phosphate from aqueous solution by biochar derived from anaerobically digested sugar beet tailings. J Hazard Mater 190:501–507. https://doi.org/10.1016/j.jhazmat.2011.03.083

Yao X, Ji L, Guo J, Ge S, Lu W, Chen Y, Cai L, Wang Y, Song W (2020) An abundant porous biochar material derived from wakame (*Undaria pinnatifida*) with high adsorption performance for three organic dyes. Bioresour Technol 318:124082. https://doi.org/10.1016/j.biortech.2020.124082

Zeng HT, Zeng HH, Zhang H, Shahab A, Zhang K, Lu YQ, Nabi I, Naseem F, Ullah H (2021) Efficient adsorption of Cr (VI) from aqueous environments by phosphoric acid activated eucalyptus biochar. J Clean Prod 286:124964. https://doi.org/10.1016/j.jclepro.2020.124964

Zessel K, Mohring S, Hamscher G, Kietzmann M, Stahl J (2014) Biocompatibility and antibacterial activity of photolytic products of sulfonamides. Chemosphere 100:167–174. https://doi.org/10.1016/j.chemosphere.2013.11.038

Zhang S, Shao T, Bekaroglu SS, Karanfil T (2010) Adsorption of synthetic organic chemicals by carbon nanotubes: effects of background solution chemistry. Water Res 44:2067–2074. https://doi.org/10.1016/j.watres.2009.12.017

Zhang XB, Guo WS, Ngo HH, Wen HT, Li N, Wu W (2016) Performance evaluation of powdered activated carbon for removing 28

types of antibiotics from water. J Environ Manag 172:193–200. https://doi.org/10.1016/j.jenvman.2016.02.038

Zhang PZ, Li YF, Cao YY, Han LJ (2019) Characteristics of tetracycline adsorption by cow manure biochar prepared at different pyrolysis temperatures. Bioresour Technol 285:121348. https://doi.org/10.1016/j.biortech.2019.121348

Zhang P, Wang X, Xue B, Huang P, Hao Y, Tang J, Maletić SP, Rončević SD, Sun H (2021a) Preparation of graphite-like biochars derived from straw and newspaper based on ball-milling and TEMPO-mediated oxidation and their supersorption performances to imidacloprid and sulfadiazine. Chem Eng J. https://doi.org/10.1016/j.cej.2021.128502

Zhang X, Chu Y, Zhang H, Hu J, Wu F, Wu X, Shen G, Yang Y, Wang B, Wang X (2021b) A mechanistic study on removal efficiency of four antibiotics by animal and plant origin precursors-derived biochars. Sci Total Environ 772:145468. https://doi.org/10.1016/j.scitotenv.2021.145468

Zhao H, Liu X, Cao Z, Zhan Y, Shi XD, Yang Y, Zhou JL, Xu J (2016) Adsorption behavior and mechanism of chloramphenicols, sulfonamides, and non-antibiotic pharmaceuticals on multi-walled carbon nanotubes. J Hazard Mater 310:235–245. https://doi.org/10.1016/j.jhazmat.2016.02.045

Zheng H, Wang ZY, Zhao J, Herbert S, Xing BS (2013) Sorption of antibiotic sulfamethoxazole varies with biochars produced at different temperatures. Environ Pollut 181:60–67. https://doi.org/10.1016/j.envpol.2013.05.056

Zheng LC, Peng D, Zhang SP, Yang YB, Zhang LJ, Meng PP (2020) Adsorption of sulfamethoxazole and sulfadiazine on phosphorus-containing stalk cellulose under different water pH studied by quantitative evaluation. Environ Sci Pollut Res 27:43246–43261. https://doi.org/10.1007/s11356-020-10241-0

Zhong J, Feng Y, Li JL, Yang B, Ying GG (2020) Removal of sulfadiazine using 3D interconnected petal-like magnetic reduced graphene oxide (MrGO) nanocomposites. Water 12:1933. https://doi.org/10.3390/w12071933

Zhou YY, Liu XC, Xiang YJ, Wang P, Zhang JC, Zhang FF, Wei JH, Luo L, Lei M, Tang L (2017) Modification of biochar derived from sawdust and its application in removal of tetracycline and copper from aqueous solution: adsorption mechanism and modelling. Bioresour Technol 245:266–273. https://doi.org/10.1016/j.biortech.2017.08.178